FEASIBILITY OF COMPLEMENTARY METAL OXIDE SEMICONDUCTOR (CMOS)-BASED TIME-OF-FLIGHT (TOF) IMAGE SENSORS IN CONJUNCTION WITH KILOVOLTAGE (KV) CONE BEAM COMPUTED TOMOGRAPHY (CBCT) FOR REAL-TIME TUMOUR TRACKING IN RADIOTHERAPY

LIM SIEW YONG @ LIM SIEW ENG

UNIVERSITI SAINS MALAYSIA

2022

FEASIBILITY OF COMPLEMENTARY METAL OXIDE SEMICONDUCTOR (CMOS)-BASED TIME-OF-FLIGHT (TOF) IMAGE SENSORS IN CONJUNCTION WITH KILOVOLTAGE (KV) CONE BEAM COMPUTED TOMOGRAPHY (CBCT) FOR REAL-TIME TUMOUR TRACKING IN RADIOTHERAPY

by

LIM SIEW YONG @ LIM SIEW ENG

Thesis submitted in fulfilment of the requirements
for the degree of
Doctor of Philosophy

March 2022

ACKNOWLEDGEMENT

I would like to express my deepest gratitude to my supervisor, Dr. Mohd Hafiz Mohd Zin, for giving me the opportunity to work on this research. With his help and guidance, I manage to perform my work more smoothly and resolve many puzzles throughout the research studies. One simply could not wish for a better supervisor.

I gratefully acknowledge MyBrain15 and Fundamental Research Grant Scheme (FRGS), from the Ministry of Higher Education (MOHE) Malaysia, for the financial support to my PhD. studies and research materials. A special gratitude goes out to staffs of Oncology and Radiotherapy Department, Advanced Medical and Dental Institute. Thanks for their help and advice on operating the system in the treatment room.

Last but not least, a special dedication to my beloved father, Mr. Lim Eng Hee and my dearest aunt, Miss Lim Kim Kee. Thank you for the love and support given that lead me overcome numerous of obstacles throughout the PhD. Journey.

TABLE OF CONTENTS

LIST OF TABLES

Page

LIST OF FIGURES

Page

LIST OF SYMBOLS

c	Speed of light
Δt	Light's propagation time
ω	Angular modulation frequency
φ	Phase shift
f	frequency
τ	Phase delay
$\otimes$	Vector product
f_{mod}	Modulation frequency
π	Mathematical constant
^{o}C	Degree Celsius
x, y	Pixel coordinate in horizontal and vertical axis

LIST OF ABBREVIATIONS

2D	Two-Dimensional
3D	Three-Dimensional
4D CT	Four-Dimensional Computed Tomography
AAPM	American Association of Physicist in Medicine
ADAS	Advanced Driver Assistant System
ASD	Average Symmetrical Surface Distance
ASU	Auto set-up
CBCT	Cone-beam Computed Tomography
CCD	Charge-Coupled Device
CMOS	Complementary Metal Oxide Semiconductor
CNR	Contrast-to-noise Ratio
CT	Computed Tomography
CTV	Clinical target volume
CW	Continuous Wave
DIBH	Deep-inspiration breath-hold
DN	Digital Number
FBP	Filtered back-projection
FIP	Fast Imaging Protocol
fps	Frame per second
FOV	Field-of-view
HU	Hounsfield unit
IARC	International Agent of Research on Cancer
ICRU	International Commission on Radiation Unit and Measurement
IGRT	Image guided radiotherapy
IMRT	Intensity-modulated radiotherapy
INU	Integral non-uniformity
IR	Infrared
kV	Kilovoltage
LCV	Low contrast visibility
LDPE	Low-density polyethylene
LED	Light-emitting diode

lp	Line pair
LUT	Look-Up Table
MNCR	Malaysian National Cancer Registry
MHz	Megahertz
MTF	Modulation transfer function
NIR	Near Infrared
PMD	Photonic Mixer Device
PMMA	Polymethyl methacrylate
PTV	Planning target volume
QA	Quality Assurance
QAP	Quality Assurance Protocol
RADAR	Radio Detection and Ranging
RGB	Red, Green and Blue, the combination colours show in the digital monitor
ROI	Region-of-Interest
RPM	Real-time Position Management
RMSE	Root mean square error
RTRT	Real-time tumour-tracking
SBI	Suppression of Background Illumination
SBRT	Stereotactic body radiotherapy
SDD	Source-to-detector distance
SGRT	Surface guided radiation therapy
SIP	Standard Imaging Protocol
SONAR	Sound Navigation and Ranging
SNR	Signal-to-Noise Ratio
TG	Task Group
ToF	Time-of-Flight
UI	Uniformity index
WHO	World Health Organisation
WP	Whole phantom Protocol
XVI	X-ray volumetric imaging

LIST OF APPENDICES

KEBOLEHLAKSANAAN PENGESAN IMEJ SEMIKONDUKTOR OKSIDA LOGAM PELENGKAP (CMOS) BERASASKAN MASA TERBANG (TOF) BERSAMA TOMOGRAFI BERKOMPUTER ALUR BERKON (CBCT) KILOVOLTAN (KV) UNTUK PENGESANAN TUMOR MASA NYATA DALAM RADIOTERAPI

ABSTRAK

Pergerakan tumor yang disebabkan oleh pernafasan merupakan salah satu sumber ketidaktentuan dalam radioterapi toraks. Pergerakan tumor secara berkala akan menyebabkan penyebaran radiasi yang kurang optimum ke kawasan tumor semasa rawatan. Objektif penyelidikan ini adalah untuk menyiasat kebolehlaksanaan dua pengesan imej Time-of-Flight (ToF) berasaskan Semikonduktor Oksida Logam Pelengkap (CMOS) dalam mengesan pergerakan tumor secara masa nyata (real-time), bersempena dengan aplikasi sistem pengimej tomografi terkomputasi sinaran kon (CBCT) yang berkuasa kilovoltage (kV). Sebuah phantom imej kualiti dinamik direka bentuk untuk mensimulasikan pergerakan pernafasan berkala pesakit. Dua pengesan imej ToF (Argos^{3D} P320 & P330, BECOM Electronics, Austria) dengan saiz susunan pixel dan jenis sumber cahaya yang berbeza digunakan dalam kajian ini. Kedua-dua pengesan imej ToF digunakan bersama dengan sistem pengimejan kV CBCT (XVI, Elekta AB, Stockholm, Sweden) untuk mengesan kedudukan dan mengkaji kualiti imej phantom dinamik. Ciri-ciri pengesan ToF diselidikkan sebelum digunakan dalam kajian. Kedua-dua pengesan imej ToF boleh mengesan kedudukan objek statik dengan ketepatan sub-milimeter. Namun demikian, prestasi kedua-dua pengesan terpengaruh kepeda kesan wiggling dan pergerakan putaran gantri mesin linac. Dua fungsi pembetulan novel diterbitkan untuk membetulkan kesilapan berkaitan dengan kesan

wiggling dan pergerakan putaran gantri. Secara purata, ketepatan pengukuran jarak dibetulkan sebanyak 96.6% bagi kesilapan demi kesan wiggling dan 90.5% untuk kesilapan berkaitan dengan putaran gantri. Pergerakan phantom berkala dengan amplitud pergerakan 1 cm hingga 3 cm diimbas dengan pengesan imej ToF dan sistem kV CBCT secara serentak. Bagi sistem pengimejan kV CBCT, dua protokal pengimejan digunalan: (i) protokol pengimejan standard (SIP) yang digunakan dalam program jaminan kualiti dan (ii) protokol pengimejan pantas (FIP_2) yang dierbitkan untuk mengurangkan artefak yang berkaitan dengan pergerakan phantom. Metrik kualiti imej yang dinilaikan adalah indeks keseragaman (uniformity index), keterlihatan kontras rendah (LCV) dan resolusi spasial (spatial resolution). Bagi ketepatan pergerakan phantom, ketepatan pengukuran menurun secara beransur-ansur apabila amplitud pergerakan meningkat. Namun demikian, walaupun pada amplitud pergerakan 3 cm, kedua-dua pengesan ToF berkebolehan untuk mengukur kedudukan sasaran dengan sisihan mutlak kurang dari 1 mm. Dari segi penilaian kualiti imej, kualiti imej CT dipengaruhi oleh pergerakan phantom yang melebihi 1 cm. Bagi protokol pengimejan SIP, imej kualiti metrik meningkat dua hingga tiga kali ganda apabila amplitud pergerakan meningkat dari 1 cm hingga 3 cm. Kualiti imej CT yang dimbas dengan protokol FIP_2 mempunyai trend peningkatan yang sama dengan protokol SIP, tetapi dengan nilai metrik kualit imej 1.5 – 1.9 kali ganda lebih tinggi. Punca utama kemerosotan imej kualiti CT adalah berkaitan rapat dengan jarak dan kelajuan pergerakan phantom. Secara kesimpulan, penyelidikan ini telah membuktikan bahawa kedua dua pengesan imej ToF berkebolehan untuk mengesan pergerakan permukaan objek dalam persekitaran bilik rawatan radioterapi. Argos^{3D} P330 mempunyai prestasi yang lebih baik dari segi ketepatan pengukuran jarak dan resolusi imej berbanding dengan Argos^{3D} P320.

FEASIBILITY OF COMPLEMENTARY METAL OXIDE SEMICONDUCTOR (CMOS)-BASED TIME-OF-FLIGHT (TOF) IMAGE SENSORS IN CONJUNCTION WITH KILOVOLTAGE (KV) CONE BEAM COMPUTED TOMOGRAPHY (CBCT) FOR REAL-TIME TUMOUR TRACKING IN RADIOTHERAPY

ABSTRACT

Respiratory induced tumour movement is one of the main causes of error in thoracic radiotherapy. The tumour movement may results in sub-optimal delivery of radiation to the target during treatment. The objective of this research is to investigate the feasibility of two Complementary Metal Oxide Semiconductor (CMOS)-based Time-of-Flight (ToF) image sensors in conjunction with kilovoltage (kV) cone-beam computed tomography (CBCT) imaging system for real-time tumour tracking in radiotherapy. A dynamic phantom was designed to simulate the periodic breathing motion of patient. Two ToF image sensors (Argos^{3D} P320 & P330, BECOM Electronics, Austria) of different pixel array size and type of illumination system were employed. The image sensors were used together with kV CBCT imaging system (XVI, Elekta AB, Stockholm, Sweden) to track the position and to assess the image quality of the dynamic phantom. The performance of the ToF image sensors were characterised prior to the application. Both ToF image sensors measure a static target position with sub-millimetre accuracy. However, both sensors were suffering from the wiggling related error and the error due to gantry rotational movement. Two novel correction functions were developed to compensate for the wiggling- and gantry rotational-related offset, respectively. On average, the distance measurement accuracy improves by 96.6% for wiggling offset and 90.5% for gantry rotational error. The periodic phantom

movements of 1 cm to 3 cm were imaged synchoronously with the ToF image sensors and kV CBCT imaging system. For kV CBCT imaging system, two imaging protocols were employed: (i) a standard imaging protocol (SIP) used in the imaging quality assurance programme and (ii) a fast imaging protocol (FIP_2) developed with the objective in reducing motion-related artefacts. The image quality metrics evaluated were the uniformity index, low contrast visibility (LCV) and spatial resolution. For phantom movement accuracy, the measurement accuracy decreases gradually as movement amplitude increases. However, even at 3 cm movement amplitude, both ToF image sensors measure the target position with a mean absolute deviation of less than 1 mm. In terms of image quality evaluation, the CT image quality is affected by the phantom movement greater than 1 cm. For SIP imaging protocol, the image quality metrics increase by two- to threefold as the movement amplitude increases from 1 cm to 3 cm. The image quality metrics acquired with FIP_2 protocol has a similar increasing trend of that obtained using SIP protocol, but with 1.5 – 1.9 times higher image quality metric values. The degradation of the CT image quality is mainly due to the moving range and the speed of the movement. In conclusion, this work has proven the feasibility of both ToF image sensors to track surface movement in radiotherapy treatment room. Argos^{3D} P330 has a better performance in terms of distance measurement accuracy and image resolution in comparison to Argos^{3D} P320.

CHAPTER 1

INTRODUCTION

1.1 Background

Lung cancer is one of the dominant cause of global death over the past fifteen years. According to World Health Organisation's International Agency for Research on Cancer (IARC), a total of 2.1 million new cases and 1.8 million cancer deaths were estimated occurred in 2018 worldwide (Bray et al., 2018). Among the new lung cancer incidence, 58.5% was reported in the Asia countries (Bray et al., 2018; Ferlay et al., 2019).

The Malaysian National Cancer Registry (MNCR) reported the number of new cases registered during the year 2012 to 2016 has reached 11,256, which is a 6.0% increase compared to the total new cases diagnosed in the past five years (2007-2011) (Abd Manan et al., 2019). Figure 1.1 shows the incidence of lung cases diagnosed in the past ten years (2007-2016). On average, there were 2200 new cases registered each year, and the prevalence of lung cancer for male and female is 69.2% and 30.8%, respectively. In terms of the survival rate, lung cancer has the lowest five years of relative survival (11%). From 2012 through 2016, lung cancer was responsible for a total of 7287 deaths in Malaysia (Malaysia, 2018). The main reason for the low survival rate is related to the late detection of the disease. As reported by MNCR, 90% of lung cancer cases were detected at stage III and IV (Malaysia, 2018). In order to reduce the number of new lung cancer and death, awareness related to lung cancer prevention and early diagnosis should be emphasised, and treatment on lung cancer should be improved.

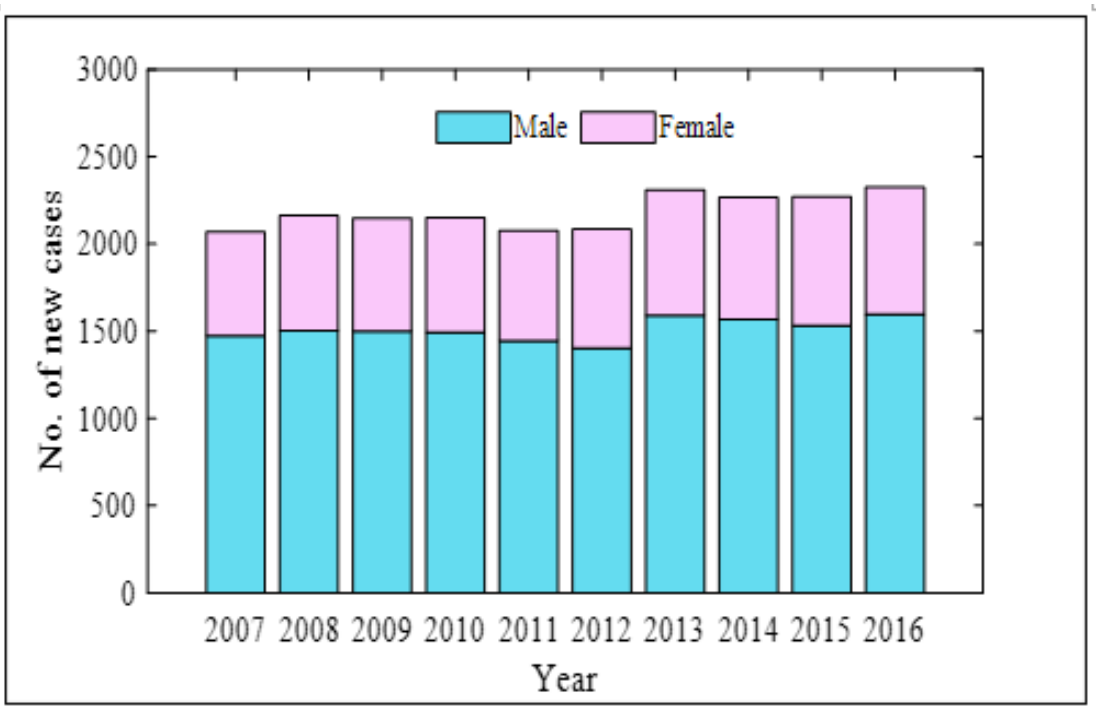

Figure 1.1 Number of new cases diagnosed during the period of 2007 to 2016. (Abd Manan et al., 2015; Abd Manan et al., 2019)

Lung cancer is categorised into two types, which are the non small cell lung cancer (NSCLC) and small cell lung cancer (SCLC). There are several ways to treat lung cancer, including surgery, chemotherapy, radiotherapy, adjuvant therapy and immunotherapy. The choice of treatment depends on the type of lung cancer and stage of cancer. In this work, we will concentrate on the advanced radiotherapy treatment and the measure to improve the treatment solution.

Radiotherapy is the cancer treatment which utilises high energy radiation beam from a linear accelerator (linac) machine to kill the cancerous cells. The primary goal of radiotherapy is to irradiate the tumour target with optimal radiation dose while minimising the damage to the neighbouring healthy tissues and critical organs. To accomplish this goal, higher precision, and effective radiation beam delivery are imperative throughout the treatment. The technological advances of radiotherapy treatment technique over the past three decades has gradually transformed the

conventional radiotherapy treatment to a more conformal and complex treatment technique such as intensity-modulated radiotherapy (IMRT) and stereotactic body radiotherapy (SBRT) (Baskar et al., 2012; Thariat et al., 2012). These advanced treatment techniques deliver higher radiation (up to 80 Gy) to tumour target with a tighter treatment margin to improve therapeutics outcome. However, there is a high potential of geographical target miss in these treatment techniques due to patient-related uncertainty, such as patient setup error and patient motion. Hence, treatment verification is highly crucial in radiotherapy and to promote better treatment verification, image-guided radiotherapy (IGRT) is introduced.

IGRT incorporates an on-board imaging device into the modern linear accelerator (linac) machine to localise tumour target and to guide targeted radiation beam during treatment (Greco et al., 2008; Thariat et al., 2012). There are various types of IGRT system, such as electronic portal imaging device (EPID), kilovoltage (kV) cone-beam computed tomography (CBCT), in-room CT scanner, ultrasound and others. Of all IGRT systems, EPID and kV CBCT based IGRT systems are the commonly used IGRT systems in the hospital (Chan et al., 2011; Cho et al., 2010; Jaffray et al., 2012). By providing planar and volumetric images, patient setup is verified via matching the bony structures of the generated two-dimensional (2D) or three dimensional (3D) image with the CT reference image. An immediate patient shift can be performed before treatment, if there is any patient setup error . Guckenberger et al. study reported that the patient setup uncertainty below 1 mm is achievable with the implementation of IGRT system (Guckenberger et al., 2007). Beyond that, Zelefsky et al. also showed that prostate cancer patient, who is treated with IGRT technique, has lower urinary toxicity and better biochemical control after radiotherapy treatment (Zelefsky et al., 2012).

However, in lung cancer treatment, patient setup variation is not the only source of error in radiotherapy planning and delivery. Tumour in the thoracic site is additionally affected by patient respiratory motion. During inspiration and expiration process, rib cage, chest wall and lungs would expand and return to their relaxed state periodically, and this, in turn, causes the cyclic displacement of the tumour target and the internal organ in all three orthogonal directions. Numerous investigations concerning the breathing induced tumour motion had been performed. As reported by Seppenwoolde et al., the respiratory induced tumour movement is the greatest in the cranial-caudal direction, and the movement range of the tumour located on the lower lobe in the lung is more significant than that in the upper lobe (Seppenwoolde et al., 2002). In American Association of Physicists in Medicine (AAPM) Task Group (TG) 76, Keall et al. also showed that the displacement of the tumour target in cranial-caudal direction is the highest of 3 mm to 22 mm, on average. Besides, the range of motion is affected by the tumour pathology and the location of the tumour (Keall et al., 2006). Due to the respiratory induced tumour motion, it is challenging to delineate tumour target, and deliver radiation dose precisely. Therefore, over the past two decades, several motion management systems or techniques are introduced to resolve the tumour motion issue. The recommended motion management systems were described in details in Chapter 2. Although various motion management techniques were recommended, such as enlarging treatment margin, using deep inspiration breath hold technique (DIBH), implementing four dimensional computed tomography (4DCT) system as well as the X-ray and optical-based tumour tracking system, respiratory induced tumour motion still remained a major challenge in radiotherapy treatment (Bertholet et al., 2019; Dhont et al., 2020).

1.2 Research Problem Statement

Breathing motion is a potential source of error in thoracic radiotherapy. As mentioned above, the breathing induced motion can range up to 22 mm in the cranial-caudal direction and require larger treatment margin to encompass the tumour motion (Keall et al., 2006; Seppenwoolde et al., 2002; Shimizu et al., 2001). Although several motion management techniques are introduced, each technique has its strength and limitation. For example, DIBH technique can effectively restrict the tumour motion and reduce the treatment margin. However, it requires patient compliance, and patient with weak lung may have difficulty in holding their breath repeatedly during treatment (Keall et al., 2006). 4DCT is a powerful imaging system that can provide a good CT image quality of a dynamic tumour and the motion range, but a good image quality result is limited to normal breathing motion only (Stine, 2015). The X-ray based tumour tracking system, like RTRT system, tracks and treat tumour motion in real-time. Nonetheless, with the implementation of fluoroscopy, the patient will be exposed to excessive radiation dose. Furthermore, the implantation of the gold surrogate may also cause the issues of pneumothorax (Harada et al., 2002; Jiang, 2006) and migration of the implanted surrogate (Shirato et al., 2003). Thus, there is a need of developing a non-intrusive image-based tracking system, which can monitor patient surface movement and internal organ motion in real-time. This study proposes the application of time-of-flight (ToF) image sensor and kV CBCT system in tracking a dynamic target. The ToF image sensor tracks the target movement, while the kV CBCT system provides the CBCT image of the dynamic target in terms of image quality metrics.

1.3 Research Objective

The primary objective of this research work is to investigate the feasibility of a commercial Complementary Metal Oxide Semiconductor (CMOS)-based ToF image sensor for real-time tumour tracking in radiotherapy, in conjunction with fast 3D kV CBCT system. To achieve the research goal, the characteristics of the ToF image sensor and the definition of fast 3D kV CBCT imaging are studied, prior to the application of both imaging system in tumour tracking. The research study is divided into four main sections which are as follows:

a) To determine the characteristics of the ToF image sensors.

b) To configure and calibrate the ToF image sensor in the treatment room and develop appropriate algorithms to correct the measurement due to environmental change.

c) To develop a set of fast CBCT imaging protocols to be used in conjuction with ToF image sensor and to characterise the resulted CBCT image quality with multiple commercial image quality phantoms.

d) To develop a dynamic phantom capable of simulating patient breathing motion as well as respiratory induced internal organ movement. To track the dynamic phantom movement with both ToF image sensor and kV CBCT system and to correlate the CBCT image quality with the target movement amplitude.

1.4 Contribution

In image-guided radiotherapy era, cone-beam CT image quality plays a vital role in the treatment verification process. The significance of the research study is the monitoring of a moving target with a cost-effective fast optical surface imaging device and

providing the image quality of the object movement quantitatively. This research work presents the operational framework of the ToF image sensor in treatment room. A set of algorithms which aims to improve the inherent wiggling error and the environment-related effect was developed. Besides, the developed dynamic phantom and a groundwork for evaluating the influence of target movement in the context of image quality may be useful in motion management quality assurance programme (QAP). Furthermore, this study also provides the findings on the correlation of the cone-beam CT image quality and the object moving amplitude.

1.5 Thesis Structure

Figure 1.2 depicts an overview of the thesis structure. This thesis comprises of seven independent chapters, as illustrated in Figure 1.2. In general, the first two chapters provide a background study of the research work. The following chapters describe the frameworks and results related to aforementioned the research objectives and the final chapter provides the summary and recommendations for future work. The following are the details of each chapter:

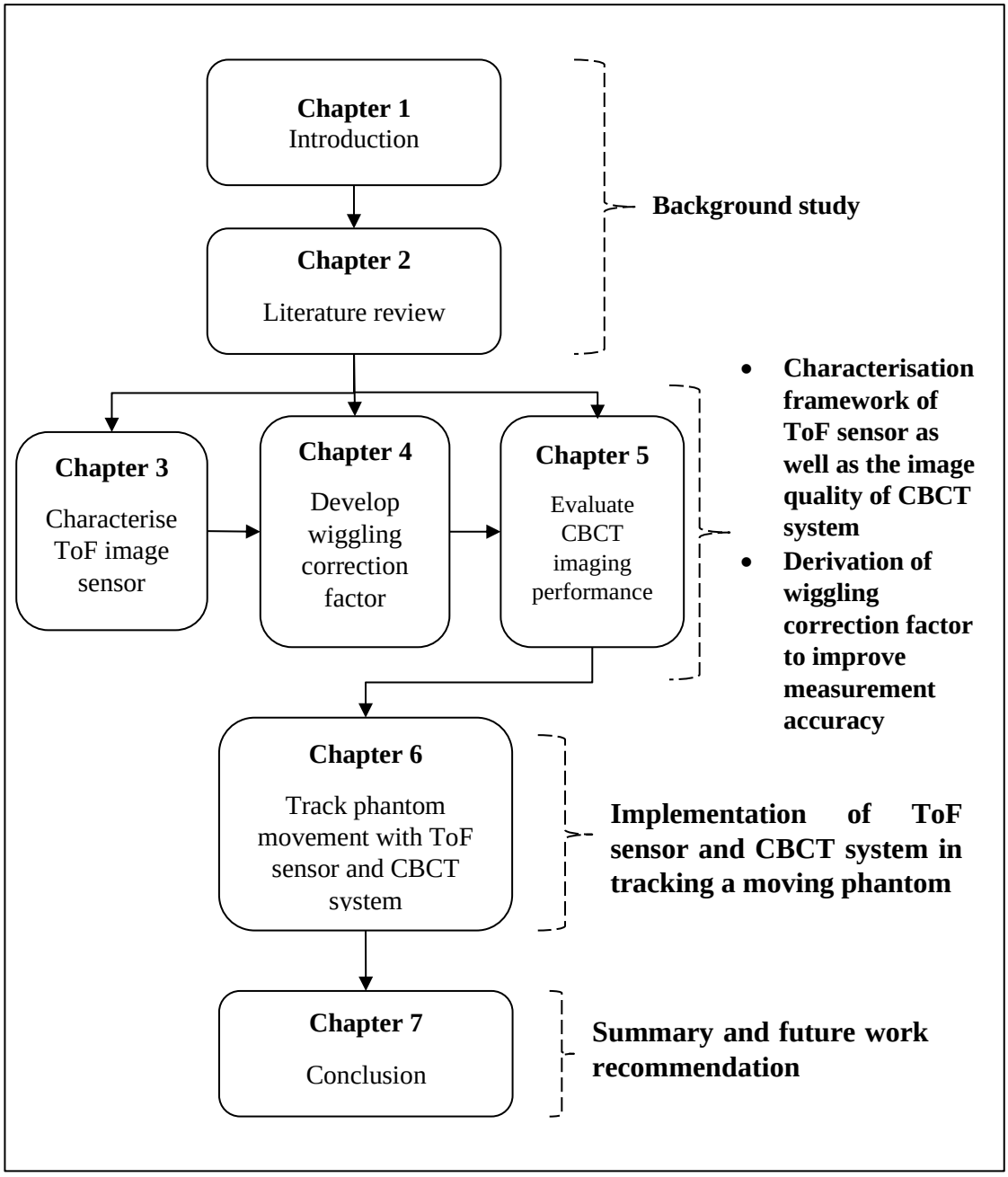

Figure 1.2 An overview of the thesis structure

Chapter 1 provides a brief overview of the breathing motion-related error in advanced radiotherapy treatment. It is followed with the problem statement, the objective and the contribution. A brief thesis structure is also included in this chapter.

Chapter 2 provides the description of various motion management techniques. Besides, the basic principles of ToF image sensor as well as the architecture and

operational method of the CMOS-based ToF image sensor are illustrated in details. The other optical surface imaging system of different working concept are studied and compared in this chapter. The advantages and the application of ToF image sensor in radiotherapy treatment verification are briefly described. In addition, a description of kV CBCT system and its applicatioin in radiotherapy treatment are presented.

Chapter 3 presents the study on the characterisation of the ToF image sensor. It starts with the specification of the ToF image sensors and the equipments used in this research study. A series of tests were performed to determine the performance of the ToF image sensors, including dark current test, warm-up time, the impact of room lights, temporal noise test, wiggling test and the distance measurement accuracy on a static object.

Chapter 4 covers the setting and calibration of the ToF image sensors in the radiotherapy treatment room. ToF image sensors are calibrated and the correction factor related to wiggling effect are developed. The methods on how the correction factor were developed is elaborated in this chapter. The motion tracking test was carried out to evaluate the efficacy of the developed correction factor as well as the performance of the ToF image sensors in tracking a target motion.

Chapter 5 describes the development of a fast imaging protocol of the kV CBCT system and the evaluation of the imaging performance. It begins with the technical specification of the kV CBCT system and the phantoms used in this work. The imaging procedure, the development of the fast imaging protocol and the determination of the image quality metrics are outlined in this chapter. The image quality results obtained using different imaging protocols were compared and discussed.

Chapter 6 presents the application of the ToF image sensor on monitoring the target movement together with kV CBCT system in real-time. Prior to the application, a correction function was developed to compensate for distance measurement offset caused by the changes in environmental or background. Then the movement of the target is recorded simultaneously with both ToF image sensor and kV CBCT system. The surface movement is determined by the ToF image sensor measurement and the image quality of the moving target is analysed with the CT data collected.

Chapter 7 summarises the findings and limits of this work, as well as the recommendation for future development.

CHAPTER 2

LITERATURE REVIEW

2.1 Introduction

Description of various respiratory motion management methods are provided in this chapter. As mentioned in Chapter 1, in order to nonintrusively monitor both surface movement and the internal motion in real-time, two different imaging systems are required: (a) optical surface imaging system and (b) kV CBCT system. With the advancement of technology, various optical surface imaging systems with various technologies and working priniciples have become available. An in-depth study on optical surface imaging technology is required to discover the potential surface imaging system for this research work.

This section starts with the overview of several respiratory motion management techniques available. This is followed by the descriptions of the fundamental concept of the Time-of-Flight imaging system as well as the architecture and the working principle of the Time-of-Flight sensor. Besides, the other well known surface imaging systems, of different operating concept, are studied and compared. In addition, in this chapter, the advantage and the application of the ToF image sensor are reported. This chapter concludes with an explanation of the working principle of kV CBCT and the its application radiotherapy treatment.

2.2 Respiratory motion management

Throughout the years, numerous respiratory motion management techniques were introduced to account for the respiratory induced intra-factional uncertainty. The motion management systems and techniques can be categorised into three main groups, including imaging technology, breath-hold technique and motion tracking system. With

the advances in imaging technology, slow CT and 4DCT are developed to account for the impact posed by the respiratory induced motion. Slow CT is the CT imaging of the tumour target using a slow gantry rotational speed (approximately 4 to 6 second per projection). The generated CT slices provide the full tumour movement due to respiration (Abdul Ghani & Ng., 2018). Meanwhile, 4DCT is the CT imaging performed with the helical or axial mode in conjunction with a respiratory tracking device, such as the abdominal belt or infrared markers. The reconstructed CT image has less motion artefacts compared to that acquired with standard CT scanner, and it gives information the tumour position at specific breathing phase. A target volume that covers the motion range can be applied in a more individualised approach to enclose the breathing motion uncertainty (Stine, 2015). The main constraint of 4DCT is that it requires longer processing time due to large image dataset (Kwong et al., 2015), and it has the problem with missing images due to the phase or amplitude sorting method (Abdul Ghani & Ng, 2018).

Apart from obtaining the motion extent through advanced imaging system, the breath-hold technique is another measure, which reduce the treatment field margin by restricting the tumour motion during radiation treatment. One of the most widely used breath-hold technique is the DIBH, where the patient is required to maintain a maximum breath-hold for 10 to 20 second during treatment. To ensure the reproducibility of the inhalation level, patient breath-hold level is monitored by a spirometer or surface imaging device. The implementation of the DIBH technique successfully reduces the tumour and internal organ movement while sparing a substantial amount of healthy lung tissue from the treatment field margin (Rosenzweig et al., 2000; Solberg et al., 2006). Forced shallow breathing technique is another motion management strategy, which provides a similar treatment outcome as DIBH technique. By using the abdominal

compression plate and stereotactic body frame, this technique reduces the diaphragmatic movement to a motion range of 5 mm to 10 mm, as the patient is still able to breathe shallowly (Cole et al., 2014; Dieterich et al., 2016; Keall et al., 2006). However, both motion management techniques required patient compliance and may introduce discomfort to the patient.

Another way of accounting for respiratory induced tumour motion is real-time tumour tracking and deliver the radiation beam as the tumour target move to a specific position. Ideally, this method can deliver the prescribed radiation dose to the target without extending the treatment volume to encompass the tumour motion, provided that the equipped tracking system can detect the tumour motion precisely. A number of studies on the real-time tracking system were published, and a few tumour tracking systems were invented and implemented clinically (Abdul Ghani et al., 2018; Kitamura et al., 2002; Stine, 2012).

The tracking systems can be divided into two types. The first type of tracking system monitors the tumour motion directly with the additional X-ray source or by detecting the surrogates implanted nearby the tumour target, such as the fluoroscopic real-time tumour-tracking system (RTRT) ((Mitsubishi Electronics Co., Ltd., Tokyo), ExacTrac® dynamic (BrainLab AG, Germany) and the Calypso® 4D localisation system (Calypso Medical Technologies, Inc, USA). In Shirato et al. study, three lung cancer patients were treated with RTRT system, and the PTV margin below 10 mm was successfully achieved (Shirato et al., 2000). However, patients who are treated with this technique would receive additional diagnostic imaging doses. According to Shirato et al., one fluoroscope in RTRT system can provide a patient a skin surface dose up to 1182 mGy per hour (Shirato et al., 2007).

Another type of tracking system, namely the optical surface tracking system, monitors patient breathing motion using an optical tracking device, and estimates the tumour position based on the breathing signal measured. The well-known surface tracking systems are the Real-time Position Management (RPM) system (Palo Alto, USA), Sentinel^{TM} Catalyst (C-Rad AB, Uppsala, Sweden) and AlignRT system (VisionRT, London, UK) (Dieterich et al., 2016; Giraud & Houle, 2013). RPM system monitors patient breathing motion with an infrared camera and gates the radiation beam at a defined breathing phase during radiotherapy treatment. A study by Ford et al. reported that eight lung and liver cancer patients were treated using the RPM system and reduced the respiratory induced uncertainty by approximately 7 mm in cranial-caudal direction (Ford et al., 2002). On the other hand, AlignRT and Catalyst track the respiratory movement of patients using two stereoscopy based cameras. The surface tracking imaging systems are connected with the treatment machine and if the patient's movement exceed a certain limit, the radiation beam would be turned off to prevent patient from futher radiation exposure. (Willoughby et al., 2012). A major challenge of AlignRT system is that it has a limited imaging speed of 10 frame per second (Halperin et al., 2019) and suffer from the occlusion of camera view due to the setting of the system (Gilles et al., 2016; Hoisak & Pawlicki, 2018).

Besides the commercially available surface tracking systems, the Time-of-Flight (ToF) image sensor, developed in year 2006, was introduced as an alternative surface tracking device. The ToF image sensor is a fast surface imaging device that provides distance information of a measured image by computing the phase difference between the emitted and reflected light signals. Several studies on patient setup verification (Gilles et al., 2016; Placht et al., 2011) and patient breathing motion tracking (Fayad et al., 2009; Wentz et al., 2012) using the Time-of-Flight (ToF) image

sensor were carried out since year 2008. In comparison to other surface tracking system, although the ToF image sensor is a compact and less complicated surface imaging device, it is innately suffered from wiggling error (described in Chapter 3).

Overall, the aforementioned respiratory motion management techniques greatly reduce treatment uncertainty caused by respiratory motion. Nevertheless, these techniques may have system limitation, involve patient compliance or even expose patient to additional radiation dose. Hence, this research aims to devise a non-invasive motion tracking system using ToF image sensor together with kV CBCT system. The study on ToF image sensor and kV CBCT system are covered in Section 2.3 and 2.7, respectively.

2.3 Time-of-Flight (ToF)

The Time-of-Flight (ToF) is a surface imaging technique that can capture a scene and provide the corresponding distance information of the target in real-time. The ToF system concept is inspired by the biological navigation skills of dolphins and bats called echolocation. Similar to echolocation, the ToF system acquires the distance details of a measured target or scene by measuring the propagation time of a signal that travels back and forth between the signal transmitter and the measured target. SONAR (sound navigation and ranging) and RADAR (radio detection and ranging) are effective ToF systems that employ sound wave and radiofrequency, respectively, to detect the distance of a measured object. These distance measurement techniques have been used for more than a hundred years, especially in the field of aeronautical and marine navigation (Bhandari et al., 2016; Teizer et al., 2007). The idea of devising an optical-based ToF system was not successful until year 2000. This is because the technology at that time was not capable of measuring the propagation time of light accurately. With the rapid

growth in the electronic field, it has been possible to realise the distance measurement with optical signals.

The optical-based ToF system is a monocular vision system. It consists of an illumination unit and an optical image sensor. The illumination unit comprises light-emitting diodes (LED) or laser diodes that actively emit infrared (IR) or near-infrared (NIR) lights with a wavelength of about 850 nm. NIR light has a wide wavelength spectral range from 700 nm to 2000 nm. The NIR light of wavelength 850 nm is imperceptible to human vision and interferes less with the natural light from the surroundings (Bamji et al., 2015; Mooney et al., 2009). Furthermore, the reflectance of most of the materials on this wavelength is comparatively higher than that of the visible light spectrum (Fang et al. 2013). Longer NIR wavelengths (>1400 nm) have a greater water absorption coefficient (Curcio & Petty, 1951) and can be easily absorbed by water and skin tissues (Tsai et al. 2017). Thus, by utilising NIR light of wavelength 850 nm, the probability of light signals loss due to absorption and transmittance is therefore minimised.

The optical image sensor is the heart of the ToF imaging system. It comprises a pixel array of photosensing unit to connvert the analogue signals into digital signals, and compute the distance value simultaneously at each pixel. Moreover, the optical sensor can accumulate the distance information, and generate a grey-scale and distance image at the same time. Hence, the optical sensor pixel is also named as ‘smart pixel’. The first “smart pixel” optical sensor was manufactured by Photonic Mixer Device (PMD) technologies, Germany, and is therefore often referred to as a PMD sensor or depth image sensor in many publications (Dal Mutto et al., 2012; Mersmann et al., 2013;

Schiller et al., 2007). Figure 2.3 displays three examples of commercial ToF imaging systems, which are widely used in a number of research studies.

Figure 2.1 The examples of the commercial ToF imaging system: (a) SwissRanger 4000™ from Mesa Imaging (Foix et al., 2011), (b) PMD Camcube 3.0 from PMD technologies (Giancola et al., 2018) and (c) Kinect V2™ from Microsoft (Ernst et al., 2015).

2.3.1 ToF working principle

The optical-based ToF imaging system captures distance information in two different approaches: (a) pulse modulation approach and (b) continuous wave (CW) modulation approach. These distance acquisition methods are associated with the illumination method and the pixel sensor architecture. The pulse modulation approach acquires the distance measurement by illuminating the scene with short light pulses. The propagation time of the light pulses is recorded at the pixel level. The distance to the target, d, is determined using Equation 2.1

$$Distance,\ d = \frac{c \times \Delta t}{2} \qquad 2.1$$

where Δt represents the light's propagation time, and c is the speed of light with a constant value of 3×10^8 ms^{-1}. This approach enables the ToF system to detect an object located at a further distance. However, the distance resolution of the ToF system is restricted by the sensor response rate and the high generation speed of the light pulses.

As reported in Luan studies, it remains a challenge for LEDs and laser diodes to generate short light pulses with a high repetition rate (Luan, 2001).

On the contrary, the CW modulation approach acquires the distance information based on the phase shift between the emitted and reflected light signals. The depth image sensor detects the modulated light signals, and extracts the phase shift by correlating the emitted and the reflected light signals. Figure 2.2 illustrates the working principle of the CW modulation approach. At first, the NIR light is modulated to generate a waveform signal by alternating the input current. A square- or sinusoidal-wave with a 10 – 100 MHz modulation frequency is generated and actively projected towards the measured scene. The emitted and detected light signals are as shown in Equation 2.2 and 2.3, respectively.

$$\textit{Emitted light signal, } g(t) = cos(\omega t)\ , \qquad 2.2$$

$$\textit{Detected light signal, } s(t) = b + a\,cos(\omega t + \varphi)\ , \qquad 2.3$$

The ω is the angular modulation frequency, where $\omega = 2\pi f$ and φ is the phase shift between the emitted and reflected light wave. The amplitude of the emitted light and the excess noise or uncertainty associated with the background illumination are denoted as a and b separately.

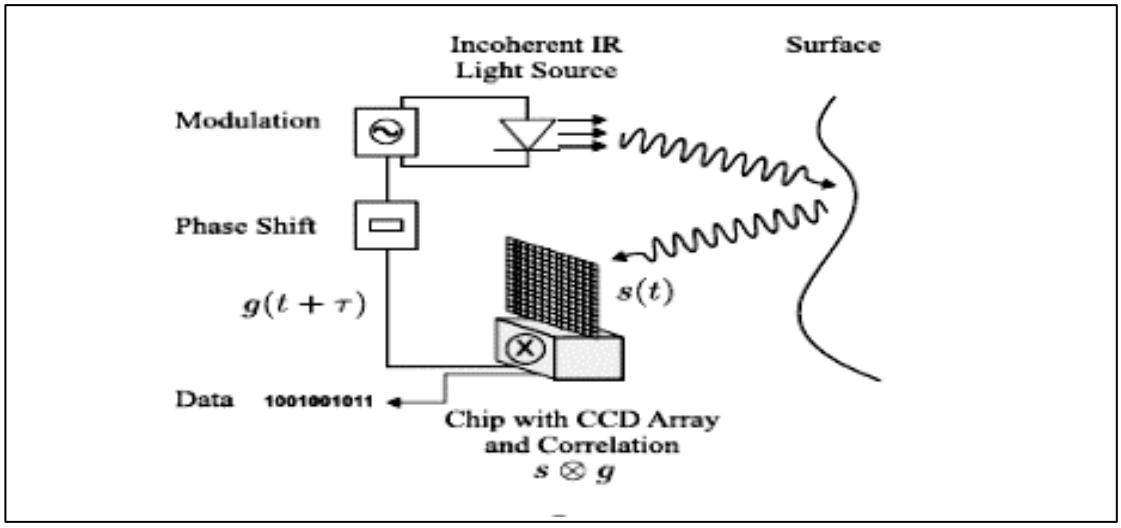

Figure 2.2 The basic working principle of the CW approach ToF system (Keller et al., 2009)

When the pixel detected the reflected signal, the pixel samples the reflected and emitted light signals for a phase delay τ. The cross-correlation function, $C(\tau)$, is formulated as shown in Equation 2.4.

$$C(\tau) = s \otimes g = \lim_{T\to\infty} \frac{1}{T} \int_{-T/2}^{T/2} s(t) \cdot g(t+\tau) dt \qquad 2.4$$

By using fundamental trigonometric calculation, the cross-correlation function is solved (see Equation 2.5), with φ as the argument of the function.

$$C(\varphi) = b + \frac{a}{2} cos(\tau + \varphi) \qquad 2.5$$

To obtain the amplitude, phase shift and signal uncertainty values, multiple sets of emitted and reflected light signal with different phase delay are acquired and sampled. As stated in Lange et al. and Giancola et al. studies, the four-bucket technique is recommended in solving the cross-correlation function (Giancola et al., 2018; Lange et al., 2001). In the four-bucket technique, the emitted and reflected signals with a phase delay of 0°, 90°, 180°, and 270° are sampled. Equation 2.6 to 2.9 show the cross-correlation function of different phase delay. In considering the effect of background signals, a K value is added to acquire the actual measured values.

$$A_0 = C(\tau_0) + K = \frac{a}{2}cos(\varphi) + K, \quad \tau_0 = 0° \qquad 2.6$$

$$A_1 = C(\tau_1) + K = -\frac{a}{2}sin(\varphi) + K, \ \tau_1 = 90° \qquad 2.7$$

$$A_2 = C(\tau_2) + K = -\frac{a}{2}cos(\varphi) + K, \ \tau_2 = 180° \qquad 2.8$$

$$A_3 = C(\tau_3) + K = \frac{a}{2}sin(\varphi) + K, \quad \tau_3 = 270° \qquad 2.9$$

Based on Equation 2.6 to 2.9, the phase shift value, φ, amplitude, a, and signal uncertainty, b, are determined (see Equation 2.10 and 2.12).

$$\varphi = tan^{-1}\left(\frac{A_3 - A_1}{A_0 - A_2}\right), \qquad 2.10$$

$$a = \frac{\sqrt{(A_3 - A_1)^2 + (A_0 - A_2)^2}}{2}, \qquad 2.11$$

$$b = \frac{A_0 + A_1 + A_2 + A_3}{4}, \qquad 2.12$$

For a sinusoidal-wave, the phase delay, τ, is given as in Equation 2.13. By substituting Equation 2.13 and 2.10 in Equation 2.1, the distance between the target and ToF sensor is calculated for a known modulation frequency (see Equation 2.14).

$$\textit{Phase delay}, \tau = \frac{\varphi}{2\pi f_{mod}}, \qquad 2.13$$

$$\textit{Distance}, d = \frac{c}{4\pi f_{mod}}\varphi = \frac{c}{4\pi f_{mod}} \cdot tan^{-1}\left(\frac{A_3 - A_1}{A_0 - A_2}\right), \qquad 2.14$$

It should be noted that the range of the measured distance is limited by the modulation frequency used. Due to the modulated light signals that vibrate periodically, the measured phase shift wraps around or restarts again for every 2π. The CW modulation

approach will generate erroneous measurement for the phase shift value greater than 2π. This condition is referred to phase wrapping ambiguity. The non-ambiguous distance, d_{namb}, or the maximum measurable distance range is determined with Equation 2.15. For a 50 MHz modulation frequency, the accessible distance is ranging from 0 to 3 m.

$$\textit{Non-ambiguous distance, } d_{namb} = \frac{c}{2f_{mod}} \qquad 2.15$$

2.3.2 The architecture and operating principle of PMD pixel

The working concept and distance calculation of the optical-based ToF surface imaging system are fully realised by the PMD sensor. Due to the rapid growth in solid-state physics, the PMD sensor chip fabrication has been moved from the charge-coupled device (CCD) technology to CMOS technology. Figure 2.3 displays an example of a PMD sensor chip PhotonICs®PMD19k (Tobias et al., 2005). With the specific pixel architecture, every pixel within the sensor is capable of performing the following operations independently:

a. Detects the reflected light signals

b. Converts optical signals to eletron charges

c. Performs cross-correlation and arithmetic estimation, and

d. Stores the accumulated electron charges.

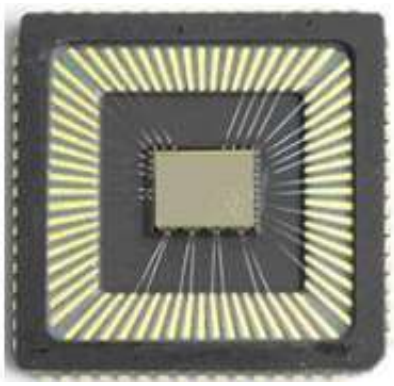

Figure 2.3 PMD sensor chip of PhotonICs®PMD19k (Tobias et al., 2005).

Over the past twenty years, various studies have been conducted to develop and implement the pixel architectures for ToF imaging system, such as the two- and four-tap photogate PMD, metal-electrode PMD, and micro-channel-plate PMD (Heredia Conde, 2017). Among the pixel designs introduced, the symmetrical two-tap photogate PMD is the most widely used pixel design for commercial PMD sensor chips (Heredia Conde, 2017; Hussmann et al., 2014; Remondino et al., 2013). Figure 2.4 (a) and (b) illustrate the cross-section and the schematic diagram of the two-tap pixel design. This pixel design comprises two photogates and two storage capacitors. As illustrated in Figure 2.4 (a), the transparent photogates are located at the centre of the pixel, which served as the modulated light signals receiver. A thin layer of silicon oxide, SiO_2, or silicon nitride, Si_3N_4, separates the transparent photogates from the p-doped substrate. There are two read-out diodes on the left and right of the photogates, connected separately to the read-out circuitry.

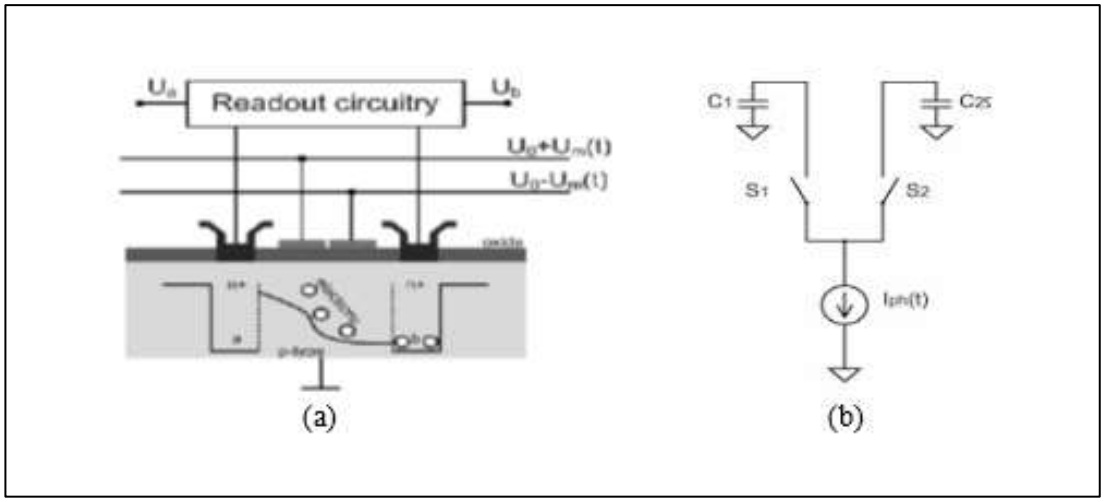

Figure 2.4 The (a) cross-section (Hussmann et al., 2014) and (b) schematic diagram (Remondino et al., 2013) of a two-tap PMD pixel.

When the modulated light signals hit the photogates, electrons are generated due to the photoelectric effect. These electrons are controlled by the push-pull voltages connected to the photogates, that transport the electrons to the storage channel on the left or right. In the cross-correlation process, the emitted signal or reference signal is connected to the photogates. If the light signal received is not modulated, the generated electrons are transported equally to channel *a* and *b*, within a modulation period. However, if the light signal detected is modulated, and the phase difference between the modulated and reference signal is 0°, the generated electrons are moved to channel *a*. If the phase difference is 180°, the electrons are drifted to channel *b* instead. The accumulated electrons in channel *a* and *b* are then read-out as voltage U_a and U_b. Figure 2.5 presents the operation of PMD pixel. In order to obtain the output voltage at each phase delay, two measurements have to be taken. The first measurement samples the output for phase delay 0° and 180°. The other measurement collects the output for phase delay 90° and 270° (Remondino et al., 2013). To eliminate background illumination, the output voltage of each phase delay is determined by Equation 2.16.

$$\textit{Output voltage, } \Delta U_{ab}(\tau) = U_a(\tau) - U_b(\tau),\ \tau = 0°, 90°, 180°, 270° \qquad \textit{2.16}$$

By substituting the output voltage of difference phase delay in Equation 2.10 and 2.14, the calculation of phase-shift value and distance can be rewritten as in Equation 2.17 and 2.18 (Hussmann et al., 2011).

$$\varphi = tan^{-1}\left(\frac{\Delta U_{ab}(270°) - \Delta U_{ab}(90°)}{\Delta U_{ab}(0°) - \Delta U_{ab}(180°)}\right), \qquad 2.17$$

$$Distance, d = \frac{c}{4\pi f_{mod}} \cdot tan^{-1}\left(\frac{\Delta U_{ab}(270°) - \Delta U_{ab}(90°)}{\Delta U_{ab}(0°) - \Delta U_{ab}(180°)}\right), \qquad 2.18$$

Overall, the PMD pixel is capable of performing the complex demodulation process consecutively at high speed and with a low power consumption. The small pixel size of 40 – 100 µm range improves the speed of the charge movement and the modulation bandwidth of the smart pixel.

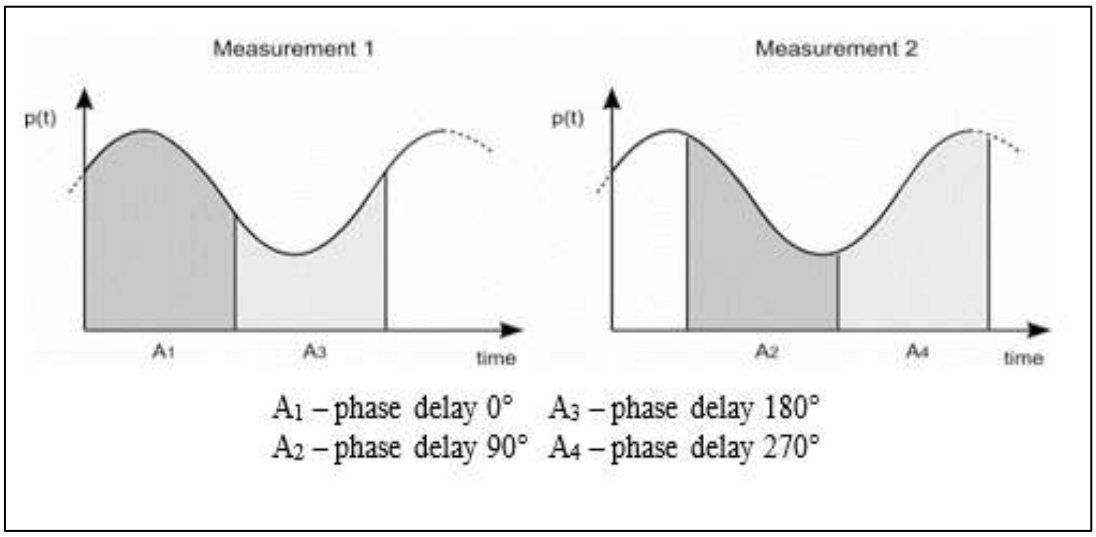

Figure 2.5 For symmetrical two-tap photogate PMD pixel, two measurements are acquired to measure the output voltage at each phase delay (Remondino et al., 2013).

2.4 Comparison of ToF system with other surface imaging technologies

Beside ToF system, stereoscopy- and structured light-base surface imaging systems are another two widely use surface imaging systems that can capture a scene image and retrieve the distance details simultaneously. The working principle of these imaging systems are completely different from the ToF surface imaging system. The difference